Emergence of a C15 Laves Phase in Diblock Polymer/Homopolymer Blends

Andreas J. Mueller, [†] *Aaron P. Lindsay,* [†] *Ashish Jayaraman,* [†] *Timothy P. Lodge,* [†,‡]

Mahesh K. Mahanthappa,[†,*] *Frank S. Bates*[†,*]

[†]Department of Chemical Engineering and Materials Science, University of Minnesota, Minneapolis, Minnesota 55455

[‡]Department of Chemistry, University of Minnesota, Minneapolis, Minnesota 55455

Corresponding Authors: bates001@umn.edu, maheshkm@umn.edu

RECEIVED DATE (to be automatically inserted after your manuscript is accepted if required according to the journal that you are submitting your paper to)

Abstract

The observation of complex, Frank-Kasper (FK) particle packings in diblock polymer melts has until recently been limited to low molecular weight, conformationally asymmetric polymers. We report temperature-dependent small-angle X-ray scattering (SAXS) studies of blends of a sphere-forming poly(styrene-*block*-1,4-butadiene) (SB) diblock polymer (M_n = 33.3 kg/mol, $Đ = M_w/M_n$ = 1.08, f_B = 0.18) with two different poly(1,4-butadiene) (B) homopolymer additives. When the B additive M_n is the same as that of the diblock core-forming B segment, these blends remarkably form tetrahedrally close-packed FK σ and Laves C14 and C15 phases with increasing B content. However, binary blends in which the B additive M_n is 60% of that of the diblock B segment form only the canonical body-centered cubic (BCC) particle packing and hexagonally-packed cylinders (HEXc). The observed phase behavior is rationalized in terms of "wet" and "dry" brush blending, whereby higher B M_n drives stronger localization of homopolymer in the particle cores while preserving the interfacial area per SB diblock chain. The consequent packing constraints in these blends destabilize the BCC packing, and FK phases emerge as optimal minimal surface solutions to filling space at constant density while maximizing local particle sphericity.

Frank-Kasper (FK) phases, a class of tetrahedrally close-packed intermetallic crystals identified in the 1950s, have become increasingly common in micellar soft materials over the past 20 years. These low symmetry, periodic crystals are characterized by large unit cells containing ≥ 7 particles of at least two distinct types with coordination numbers CN = 12, 14, 15, or 16.[1,2] Studies of sphere-forming thermotropic liquid crystalline dendrons[3–5] and giant shape amphiphiles,[6–8] Type I ("normal") aqueous lyotropic liquid crystals (LLCs),[9,10] and low molecular weight (M) diblock polymer melts[11,12] have revealed a common phase progression from a body-centered cubic (BCC) packing to FK σ and A15 phases with increasing micelle core composition. These soft FK phases are characterized by spontaneous formation of two or more symmetry-equivalent particle classes of discrete sizes that vary by up to ±10% around a mean value, and which occupy sites of different CN in the lattice. These structures ostensibly represent optimal minimal surface solutions to filling space at constant density when the micelle core/corona interfacial area becomes substantial.[13–17] A significant outlier to this trend is the nearly exclusive formation of C15 phases with $Fd\bar{3}m$ symmetry in Type II ("inverse") aqueous LLCs,[18–20] comprising nanoscale pools of water in a hydrocarbon matrix, albeit with some exceptions.[21–23] Note that the cubic C15 and related 3D-hexagonal C14 ($P6_3/mmc$ symmetry) phases represent a sub-class of FK structures known as Laves phases, which exhibit only CN = 12 and 16 sites.

Experiments have only recently established that both C14 and C15 Laves phases form in diblock polymers and in oil-swollen aqueous Type I LLCs. Kim et al. found that specific thermal processing protocols enable access to metastable C15 and C14 phases in low-M diblock polymer melts.[24] Shortly thereafter, Baez-Cotto and Mahanthappa reported that *n*-decane localization in the micelle cores of Type I aqueous LLCs of a hydrated decanoate (C_{10}) surfactant apparently drives equilibrium C15 and C14 Laves phase formation.[25] In the latter case, particle size speciation occurs by surfactant and oil redistribution to access the requisite discrete particle size distribution, exhibiting ±20% variation around the mean volume. Here, we extrapolate these findings to analogous homopolymer/diblock blends. Note that the σ phase (with CN = 12, 14, and 15 sites) has, until recently,[26] only been observed in conformationally asymmetric, low-M diblocks,[27] and FK phases are entirely absent in single-component

high-*M* poly(styrene)-*block*-poly(1,4-butadiene) (SB) materials.[28] Herein we demonstrate that judiciously designed blends of a sphere-forming (SB) diblock copolymer with poly(1,4-butadiene) homopolymer (B) enable access to self-assembled FK σ and Laves C14 and C15 phases. These findings provide initial insights into scale-invariant principles that underlie symmetry selection amongst these nearly energetically-degenerate micellar FK phases.[24]

Although the effects of homopolymer addition on the morphologies of diblock melts have been reported,[29–38] notably adding homopolymer to the corona blocks in spherical structures,[39,40] detailed studies of the phases arising from swelling sphere-forming diblock cores with homopolymer have not appeared to the best of our knowledge. Theory suggests that, if homopolymer added to minority diblock segment domains is excluded from the diblock interdomain interface, higher mean interfacial curvature structures (i.e., particle-based phases) will be favored, running counter to the trend towards lower mean interfacial curvature structures encountered by increasingly symmetric neat diblocks.[41,42] The extent of this exclusion is regulated by a mixing-entropy-based drive for homogenous homopolymer solubilization, which vanishes for sufficient homopolymer degree of polymerization (N_{homo}).[43] This regime is referred to as the dry-brush limit, and has been experimentally shown to occur in AB/B systems when the ratio of $N_{B,homo}$ to the corresponding diblock-segment $N_{B,diblock}$ approaches unity ($\alpha = N_{B,homo}/N_{B,diblock} \approx 1$).[44–46] This situation is directly analogous to that of the oil localization in the aforementioned Type I LLCs with matched oil and surfactant carbon numbers.[25,47]

To test whether high-*M* SB/B blends with $\alpha \approx 1$ recapitulate the phase behavior of oil-swollen Type I aqueous LLCs, we used living anionic polymerization to synthesize a narrow dispersity diblock SB-18 with $M_n = 33.3$ kg/mol, $Đ = M_w/M_n = 1.08$, and B block volume fraction $f_B = 0.18$, and a narrow dispersity poly(1,4-butadiene) homopolymer additive B-6 with $M_n = 5.7$ kg/mol ($Đ = 1.08$) for blend morphology studies (see Supporting Information for synthesis and molecular characterization details in Table S1 and Figures S1–S2). Temperature-dependent synchrotron small-angle X-ray scattering (SAXS) analyses establish that SB-18 orders into a BCC phase with a lattice parameter $a = 25$ nm (see Figure S3) at 120 °C and that it is disordered at $T \geq 150$ °C. Polymer blends were prepared by co-dissolving SB-18, B-6,

and 0.2 wt% BHT (an antioxidant that does not affect phase behavior at this concentration)[26] in benzene, followed by freeze-drying. To minimize thermal oxidative degradation, samples were hermetically sealed into aluminum DSC pans under argon for synchrotron SAXS analyses (see Supporting Information for details). Blends were thermally annealed at 200 °C for < 30 min, above the order-disorder transition of many of the blends, prior to subsequent extended annealing at a specific $T \leq 200$ °C for 24–60 h to facilitate ordered melt microphase separation. We emphasize that no degradation was observed under these conditions as evidenced by color changes or increases in $Đ$, consistent with past studies of SB.[26] Binary SB18/B-6 blends are parameterized by the diblock volume fraction in the blend (ϕ_{SB}), from which the net B volume fraction in the blend ($f_{B(tot)}$) was calculated.

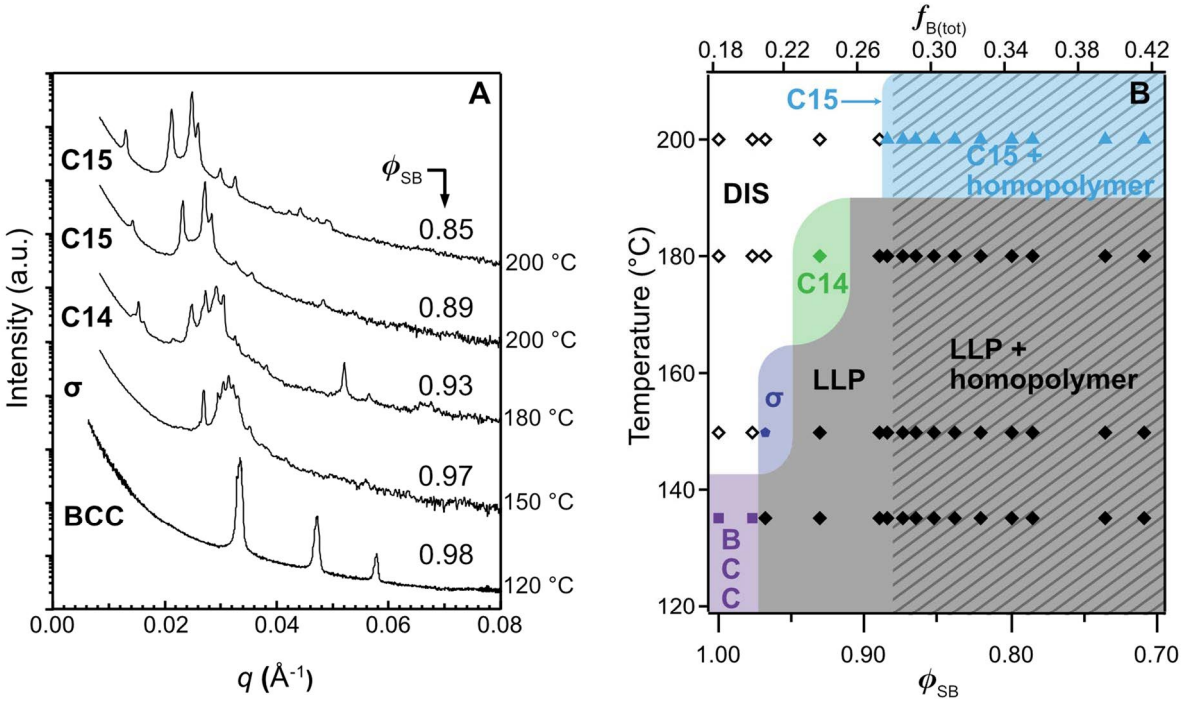

Figure 1. (A) Representative synchrotron SAXS intensity ($I(q)$) versus scattering wavevector (q) profiles for various, thermally annealed SB-18/B-6 blends with $\alpha = 1.08$ as a function of ϕ_{SB}, at the indicated temperatures. (B) Experimental phase portrait for SB-18/B-6 blends, in which the hatched region corresponds to macrophase separated blends.

SAXS powder patterns presented in Figure 1A reveal that SB-18/B-6 blends ($\alpha = 1.08$) microphase separate into four different ordered morphologies with decreasing ϕ_{SB} (increasing B-6 additive content). The blend with $\phi_{SB} = 0.98$ adopts a slightly swollen BCC structure with lattice parameter $a = 27$ nm at

120 °C, as compared to a = 25 nm for neat SB-18 at the same temperature. Contrary to the sphere-to-cylinder transition at $f_B \approx 0.20$ expected for the neat diblock,[28] the blend with $\phi_{SB} = 0.97$ and $f_{B(tot)} = 0.20$ exhibits the distinctive scattering signature of a tetragonal FK σ phase with $P4_2/mnm$ symmetry and lattice parameter a = 88.2 nm with c/a = 0.531 (see Figure S4 and Table S2 for pattern indexing). The spotty and somewhat anisotropic 2D-SAXS pattern (see Figure S5A) for this blend suggests a high degree of long-range translational order; this results in an azimuthally-integrated 1D-SAXS intensity profile with less sharp peaks than reported previously based on powder patterns with isotropic diffraction rings. Decreasing the SB-18 content in the blend to $\phi_{SB} = 0.93$ with $f_{B(tot)} = 0.23$ furnishes a complex scattering pattern consistent with a C14 Laves phase with $P6_3/mmc$ symmetry and a = 50.9 nm and c = 82.2 nm (see Figure S6 and Tables S3–S4 for indexing) with a nearly ideal c/a = 1.615. The anisotropic nature of the 2D-SAXS patterns for this sample, including the appearance of Bragg rods (streaks in Figure S5B), suggests the presence of stacking faults in the structure.[48] Hexagonal C14 (AABBAABB… stacking) and cubic C15 (AABBCCAA… stacking) Laves phases are crystallographically related by stacking defects, such that the (002) Miller plane of the C14 structure is epitaxially related to the (111) plane of the C15 phase.[49] Thus, the prominent intensity of the second peak corresponding to the C14 (002) reflection is consistent with the stacking fault hypothesis as well as possible C15 phase coexistence (see Figure S6). Finally, blends with ϕ_{SB} = 0.87–0.89 ($f_{B(tot)}$ = 0.26-0.28) form well-ordered C15 Laves phases with $a \approx 84$ nm as evidenced by the indexed SAXS pattern presented in Figure 2A, which exhibits the first 15 expected reflections for the $Fd\bar{3}m$ symmetry (see Figure S5C and S5D for 2D-SAXS patterns, and Table S5 for peak positions and residuals). Per a previously established methodology,[10,12,50] we extracted the structure factor intensities from this SAXS powder pattern in Figure 2A by Le Bail refinement[51] and used the *SUPERFLIP* charge flipping algorithm[52] to reconstruct the electron density maps (90% isosurface) shown in Figures 2B and 2C (see Supporting Information for details). The topologies of these electron density maps resemble those of previously reported C15 phases, and they provide a qualitative sense of the

distinctly aspherical geometries and bimodal size distributions required of particles that spontaneously form in this ordered morphology.

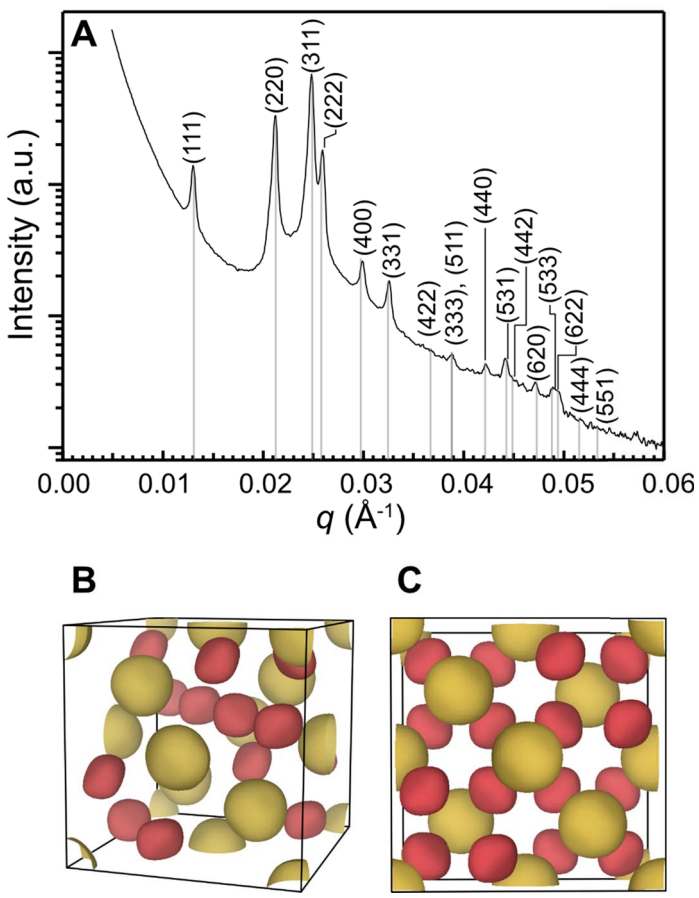

Figure 2. (A) Synchrotron SAXS pattern for the α = 1.08 SB-18/B-6 blend at ϕ_{SB} = 0.85, acquired after annealing the sample for 24 h at 200 °C. Indexing lines and matching Miller indices correspond to a cubic C15 Laves phase ($Fd\bar{3}m$ symmetry) with unit cell parameter a = 84 nm. (B) Electron density reconstruction (90 % isosurface) generated from the 1D-SAXS profile using a charge flipping algorithm (see text for details). Two symmetry-equivalent particles are evident, occupying the *8a* (*gold*) and *16d* (*red*) Wyckoff positions. (C) Electron density map looking down the [100] direction.

Decreasing to ϕ_{SB} < 0.87 results in no change in the C15 unit cell parameter (Figure S7) and these samples exhibit a hazy appearance, observations consistent with B-6 macrophase separation from the homopolymer-swollen C15 Laves structure. Instead of exhibiting a sphere-to-cylinder transition with increasing $f_{B(tot)}$, SB/B blends with α = 1.08 form spherical particle morphologies even at $f_{B(tot)}$ = 0.28. The phase behavior of these SB-18/B-6 blends are summarized in the phase portrait given in Figure 1B.

Blend microphase separation into FK phases when $\alpha = 1.08$ is accompanied by a substantial thermal activation barrier for phase nucleation and growth, evidenced by the prevalence of a disorganized, liquid-like packing (LLP) of particles when $T \leq 180$ °C (Figure 1B). This LLP state differs from a disordered melt (DIS), as the LLP is characterized by a strong principal SAXS peak and subtle scattering features consistent with short-range interparticle correlations in a segregated melt (Figure S9). This thermal activation barrier, which may be overcome by extended high temperature annealing, stems partially from the barriers for homopolymer and diblock chain exchange between micelles to form the requisite discrete distributions of 5, 3, or 2 distinct sphere sizes required for σ, C14, or C15 phase formation, respectively.[24] The rates of diblock chain exchange are extremely temperature sensitive due to their scaling as $\exp(-\chi N_{SB})$, where the effective segmental interaction parameter $\chi \sim T^{-1}$.[53,54] Homopolymer mass redistribution amongst the segregated micelle cores is also likely slow, as these chains incur substantial energetic penalties associated with expulsion from the micelle cores and transit through the chemically dissimilar corona domains.

In order to assess the role of B homopolymer additive M_n on blend phase behavior, we prepared blends with $\alpha = 0.60$ from SB-18 and a narrow dispersity B-3 homopolymer with $M_n = 3.2$ kg/mol ($Đ = 1.09$). 1D-SAXS intensity profiles associated with these binary blends are given in Figure 3A, along with a summary of the observed phase behavior in Figure 3B. With decreasing ϕ_{SB}, we observe only the canonical BCC and HEXc morphologies. When $\phi_{SB} = 0.94$, the obtained swollen BCC phase exhibits a lattice parameter $a = 28$ nm (Figure 3A). The weaker primary reflection and lack of higher order Bragg peaks in this pattern suggest limited long-range order. This observation is consistent with the expected melt compatibilization by the addition of low-M homopolymer that drives the system towards disorder,[43] an inference further supported by the absence of any ordered structures when $\phi_{SB} = 0.94$–0.98. When $0.90 \geq \varphi_{SB} \geq 0.73$, SAXS analyses reveal the 2D-hexagonal order of a HEXc morphology (Figure 3A). Variations in the intensities of certain higher order reflections may be explained in terms of volume fraction-dependent form factor extinctions (see Figure S10). Moreover, the principal HEXc scattering

peak (q^*) systematically shifts to lower q-values with increasing B-3 loading, signifying swelling of the cylindrical microstructure with added homopolymer, in sharp contrast to the finite miscibility of the B-6 additive in the C15 phase of the α = 1.08 blends.

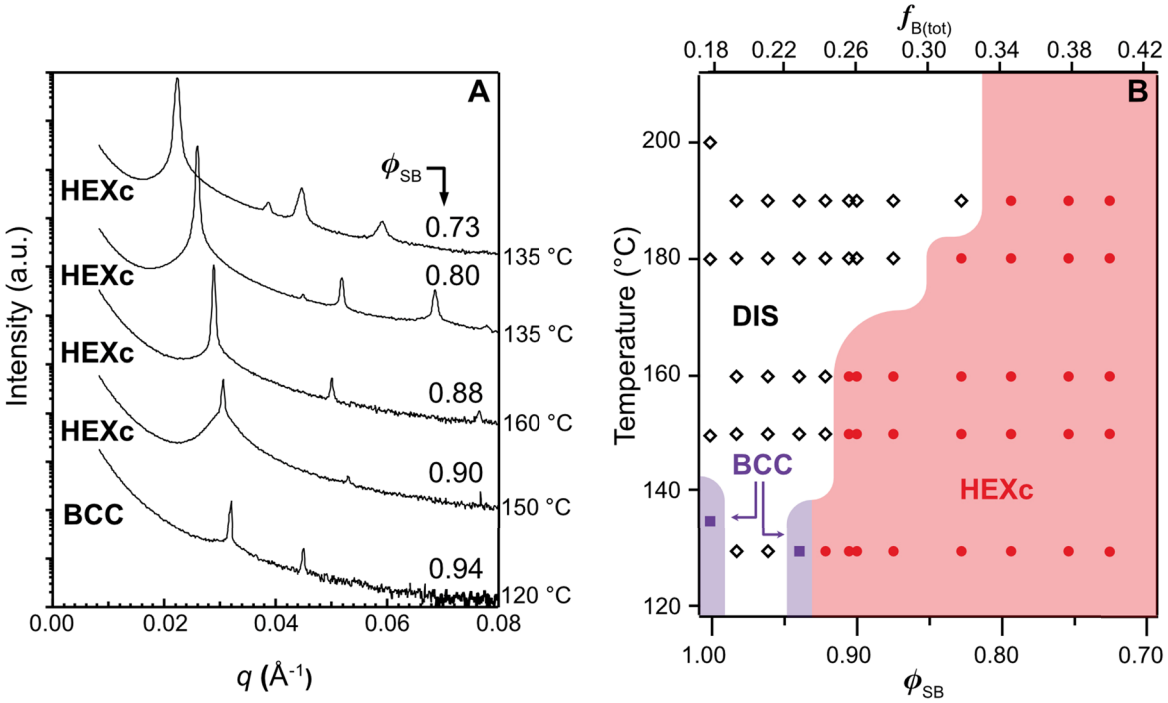

Figure 3. Phase behavior of the α = 0.6 SB-18/B-3 blend: (A) Representative synchrotron SAXS powder patterns of blend with various ϕ_{SB} that were annealed for 24-60 h at the indicated temperatures, and (B) a portrait of the experimentally observed phase behavior.

The homopolymer-driven evolution of particle size shown in Figure 4 further underscores differences between the "dry brush" (α = 1.08) and "wet brush" (α = 0.60) blends. Average particle radii were calculated from the average volume per spherical particle, using the SAXS-derived unit cell volumes. The α = 0.60 blend in Figure 4B is characterized by a monotonic increase in particle size with increasing B homopolymer (decreasing ϕ_{SB}) until φ_{SB} = 0.73, with an expected discontinuity at the transition from spheres to HEXc accompanying the sharp decrease in mean interfacial curvature. Extraordinarily, simply increasing homopolymer molecular weight by 2.5 kDa as in the α = 1.08 blend completely erases any sphere-to-cylinder order-order transition in the blends. A monotonic increase in particle size is instead observed down to $\phi_{SB} \approx 0.87$, after which particle size saturates (Figure 4A) and macrophase separation occurs (Figure 1B).

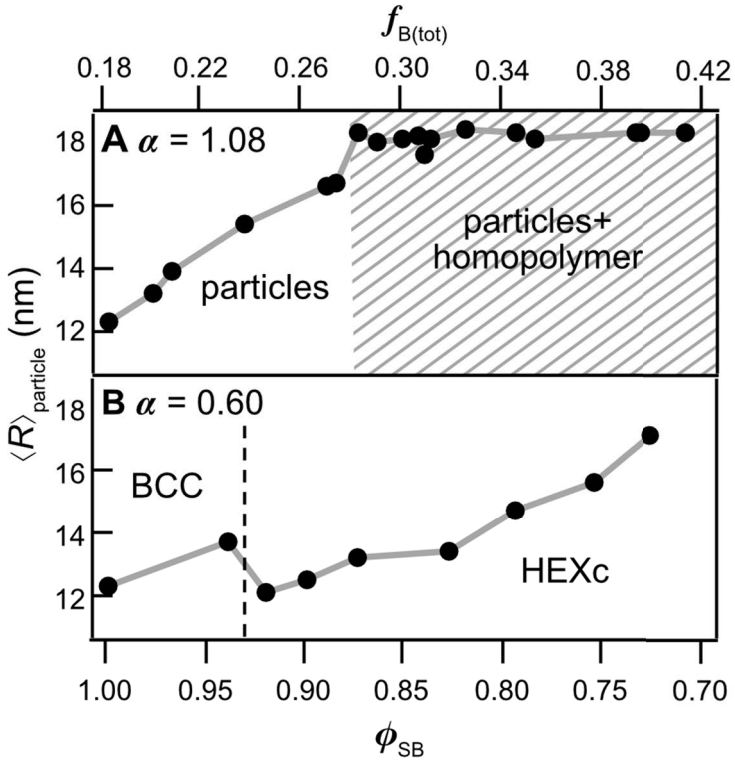

Figure 4. Evolution of average particle radius with ϕ_{SB} in SB/B blends with (A) α = 1.08 indicating monotonically increasing sphere size until the onset of B additive macrophase separation (hatched region), and (B) α = 0.60, in which the discontinuity corresponds to the BCC to HEXc transition.

The divergent phase behaviors of the α = 1.08 and α = 0.60 blends apparently stem from differences in how B homopolymer localizes within microphase separated particles, as depicted in Figure 5. Blends of α = 0.60 most likely conform to a "wet brush" model, wherein homopolymer swells the initially spherical diblock domains (Figure 5A,B) uniformly, driving an increase in interfacial area per diblock and consequently a decrease of mean interfacial curvature exemplified by the formation of HEXc (Figure 5C).[44–46] Conversely, blends of $\alpha \approx 1$ likely conform to a "dry brush" model, wherein homopolymer exclusion from the S/B interface drives strong B additive localization in the areas of intense packing frustration at the particle centers.[44–46] The interfacial area per diblock chain in these blends is preserved, which instead drives formation of high mean curvature, spherical particle phases (Figure 5D) until the onset of homopolymer macrophase separation as in the α = 1.08 blend.

Irrespective of mesoscale segmental arrangements, diblock polymer melts are subject to the constraint of filling space at constant monomer density imposed by maximizing van der Waals cohesion between

individual chains. Therefore, any arrangement of discrete micelles must partition space at uniform density, requiring particles to deform from their optimal spherical shape into polyhedral Wigner-Seitz (WS) cells, which reflect the lattice site coordination environments within the microphase separated structure (Figures 5A and 5B). Dry brush homopolymer swelling of the truncated octahedra which partition space in a BCC lattice ultimately leads to an amplified imprinting of the coronal WS cell boundary onto the S/B interface,

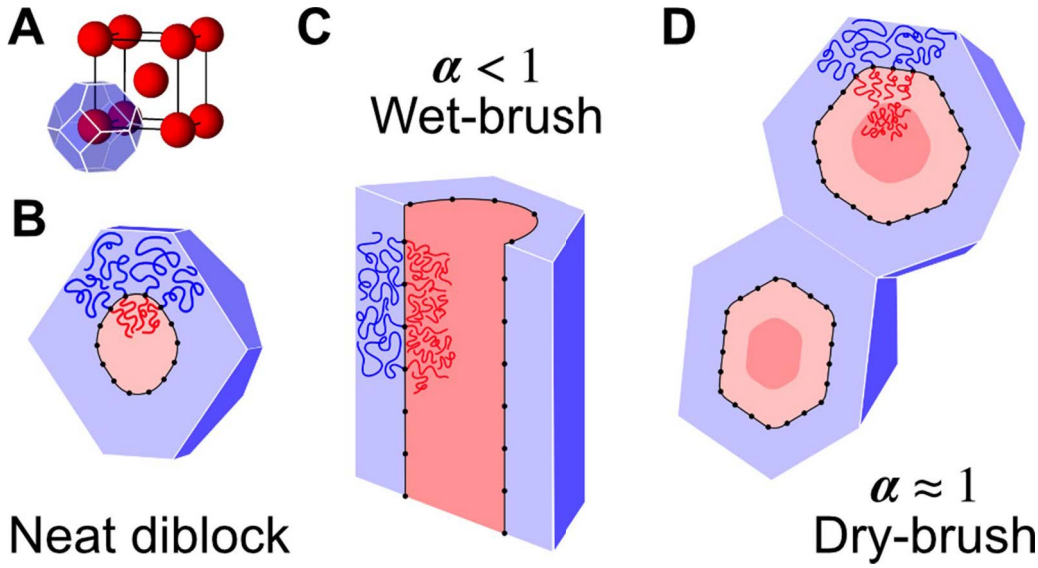

Figure 5. (A) Illustration of a BCC unit cell formed by the neat SB-18 diblock melt with the Wigner-Seitz (WS) cell shown at one position. (B) (110)-slice of the WS cell in part A. (C) Slice of cylindrical micelle comprising HEXc after B-3 homopolymer addition (α = 0.60). Dark red areas represent presumed B localization. Note the delocalization of homopolymer within the core and the spreading out of black diblock junction points, reflecting the homopolymer-induced increase of diblock interfacial area per chain, leading to a flattening of the interface. (D) (110)-slice of the 2 different WS cells comprising C15 after saturation with B-6 homopolymer in the α = 1.08 blends. Note homopolymer localizing far from the interface, preserving diblock interfacial area per chain.

as the diblock chains that decorate the homopolymer core relax. This polyhedral warping of the interface leads to an increased penalty due to interfacial tension, thus triggering a transition to a lattice with greater average spherical particle character (Figure 5D). Indeed, current explanations of FK phase formation in neat diblock melts ascribe the preferential formation of the σ phase to its high average particle sphericity, as that structure simultaneously minimizes chain stretching and interfacial area relative to BCC.[15,17] In contrast, the remarkable 20% volume variation about the mean between constituent particles[24] means that the Laves phases exhibit considerably greater packing frustration than FK σ and A15 phases, wherein the volume differences between particles are less than 10 %. However, the diblock foam model recently

developed by Reddy et al. indicates that the Laves C14 and C15 phases represent minimal surface solutions to tiling 3D space at constant density, albeit with a low degree of packing frustration.[17] Accordingly, we posit that minority block homopolymer addition serves to allow volume relaxation-based pathways to the minimal surface C14 and C15 structures by relieving the core packing-frustration that otherwise restricts their formation. Related blends of SB-13 (M_n = 31.0 kg/mol, $Đ$ = 1.08, f_B = 0.125) with B-3 and with B-2 (M_n = 2.1, $Đ$ = 1.1) that exhibit α = 0.95 and 0.65, respectively, demonstrate the same α-dependent C15 or HEXc formation (Figures S11 and S12) in further support of these ideas. In fact, Uddin et al. may have inadvertently established these concepts in low-*M* systems in the early 2000s through their observation of a C15 phase in ultra-low molecular weight poly(oxyethylene)-poly(dimethylsiloxane).[55,56] Although they physically rationalize their unexpected observation as deriving from a neat melt, their diblock oligomers were only 93 wt% pure with 7 wt% core homopolymer impurity– a low molecular weight diblock/core homopolymer blend that forms the same complex phases reported here. Self-consistent field theory applied to miktoarm star copolymers that form σ or A15 phases shows that addition of homopolymer to the paticle cores can result in the C14 and C15 Laves phases.[57] Taken together with data from oil-laden Type I LLCs and Type II LLCs, these findings indicate that Laves phases are a general feature in micellar materials with relatively soft cores.

In summary, we have studied the morphologies of blends of a high-*M*, BCC-forming SB-18 diblock polymer with B homopolymers of two different molecular weights such that α = 1.08 and α = 0.60, respectively. While the α = 0.60 blends form only BCC and HEXc morphologies, the α = 1.08 blend exhibits remarkably divergent phase behaviors at the same overall $f_{B(tot)}$ including adoption of well-ordered FK σ and Laves C14 and C15 particle packings. These findings establish a simple strategy for producing complex micellar packings at long length scales based on high-*M* diblocks, by direct analogy to phenomena observed in low-*M* surfactant LLCs. We anticipate that these findings will provide a foundation for constructing far-reaching geometric design principles for scale-invariant, mesoscopic soft matter self-assembly.

ASSOCIATED CONTENT

Supporting Information

The Supporting Information is available free of charge at: [inset url]

Experimental details and additional characterization data (PDF)

AUTHOR INFORMATION

Corresponding Authors

Mahesh K. Mahanthappa − *Department of Chemical Engineering and Materials Science, University of Minnesota, Minneapolis, Minnesota 55455, United States*; orcid.org/0000-0002-9871-804X; Email: maheshkm@umn.edu

Frank S. Bates − *Department of Chemical Engineering and Materials Science, University of Minnesota, Minneapolis, Minnesota 55455, United States*; orcid.org/0000-0003-3977-1278; Email: bates001@umn.edu

Authors

Andreas J. Mueller − *Department of Chemical Engineering and Materials Science, University of Minnesota, Minneapolis, Minnesota 55455, United States*; orcid.org/0000-0002-4750-480X

Aaron P. Lindsay − *Department of Chemical Engineering and Materials Science, University of Minnesota, Minneapolis, Minnesota 55455, United States*; orcid.org/0000-0003-0223-193X

Ashish P. Jayaraman − *Department of Chemical Engineering and Materials Science, University of Minnesota, Minneapolis, Minnesota 55455, United States*; orcid.org/0000-0001-7071-7419

Timothy P. Lodge − *Department of Chemical Engineering and Materials Science and Department of Chemistry, University of Minnesota, Minneapolis, Minnesota 55455, United States;*

orcid.org/0000-0001-5916-8834

Notes

The authors declare no competing financial interest.

ACKNOWLEDGMENTS

We thank Ronald Lewis, III for providing the diblock copolymers utilized in this study. Financial support for this work was under National Science Foundation grants DMR-1801993 (A.J.M., F.S.B.) and CHE-1807330 (A.J., M.K.M.), and a National Science Foundation Graduate Research Fellowship under Grant No. 00039202 (A.P.L.). SAXS experiments were conducted at the Advanced Photon Source (APS), Sector 5 DuPont-Northwestern-Dow Collaborative Access Team (DND-CAT). DND-CAT is supported by E.I. DuPont de Nemours & Co., the Dow Chemical Company, and Northwestern University. Additional SAXS experiments were also carried out at Sector 12 of the APS. Use of the APS, an Office of Science User Facility operated for the U.S. Department of Energy (DOE) Office of Science by Argonne National Laboratory, was supported by the U.S. DOE under Contract No. DE-AC02-06CH11357. Parts of this work, including lab source SAXS analyses, were carried out in the Characterization Facility at the University of Minnesota, which receives partial support from NSF through the UMN MRSEC (DMR-1420013).

REFERENCES

(1) Frank, F. C.; Kasper, J. S. Complex Alloy Structures Regarded as Sphere Packings. I. Definitions and Basic Principles. *Acta Crystallogr.* **1958**, *11*, 184–190.

(2) Frank, F. C.; Kasper, J. S. Complex Alloy Structures Regarded as Sphere Packings. II. Analysis and Classification of Representative Structures. *Acta Crystallogr.* **1959**, *12*, 483–499.

(3) Ungar, G.; Liu, Y.; Zeng, X.; Percec, V.; Cho, W. D. Giant Supramolecular Liquid Crystal Lattice. *Science.* **2003**, *299*, 1208–1211.

(4) Zeng, X.; Ungar, G.; Liu, Y.; Percec, V.; Dulcey, A. E.; Hobbs, J. K. Supramolecular Dendritic Liquid Quasicrystals. *Nature* **2004**, *428*, 157–160.

(5) Percec, V.; Peterca, M.; Tsuda, Y.; Rosen, B. M.; Uchida, S.; Imam, M. R.; Ungar, G.; Heiney, P. A. Elucidating the Structure of the Pm3̄n Cubic Phase of Supramolecular Dendrimers through the Modification of Their Aliphatic to Aromatic Volume Ratio. *Chem. Eur. J.* **2009**, *15*, 8994–9004.

(6) Huang, M.; Hsu, C.-H.; Wang, J.; Mei, S.; Dong, X.; Li, Y.; Li, M.; Liu, H.; Zhang, W.; Aida, T.; Zhang, W. B.; Yue, K.; Cheng, S. Z. D. Selective Assemblies of Giant Tetrahedra via Precisely Controlled Positional Interactions. *Science*. **2015**, *348*, 424–428.

(7) Yue, K.; Huang, M.; Marson, R. L.; Hec, J.; Huang, J.; Zhou, Z.; Wang, J.; Liu, C.; Yan, X.; Wu, K.; Guo, Z.; Lui, H.; Zhang, W.; Ni, P.: Wesdemiotis, C.; Zhang, W. B.; Glotzer, S. C.; Cheng, S. Z. D. Geometry Induced Sequence of Nanoscale Frank-Kasper and Quasicrystal Mesophases in Giant Surfactants. *Proc. Natl. Acad. Sci. U. S. A.* **2016**, *113*, 14195–14200.

(8) Su, Z.; Hsu, C.; Gong, Z.; Feng, X.; Huang, J.; Zhang, R.; Wang, Y.; Mao, J.; Wesdemiotis, C.; Li, T.; Seifert, S.; Zhang, W.; Aida, T.; Huang, M.; Cheng, S. Z. D. Identification of a Frank-Kasper Z Phase from Shape Amphiphile Self-Assembly. *Nat. Chem.* **2019**, *11*, 899–905.

(9) Vargas, R.; Mariani, P.; Gulik, A.; Luzzati, V. Cubic Phases of Lipid-The Structure of Phase Q223 (Space Group Pm3n). An X-Ray Scattering Study. *J. Mol. Biol.* **1992**, *225*, 137–145.

(10) Kim, S. A.; Jeong, K. J.; Yethiraj, A.; Mahanthappa, M. K. Low-Symmetry Sphere Packings of Simple Surfactant Micelles Induced by Ionic Sphericity. *Proc. Natl. Acad. Sci. U. S. A.* **2017**, *114*, 4072–4077.

(11) Lee, S.; Bluemle, M. J.; Bates, F. S. Discovery of a Frank-Kasper σ Phase in Sphere-Forming Block Copolymer Melts. *Science.* **2010**, *330*, 349–353.

(12) Bates, M. W.; Lequieu, J.; Barbon, S. M.; Lewis, R. M.; Delaney, K. T.; Anastasaki, A.; Hawker, C. J.; Fredrickson, G. H.; Bates, C. M. Stability of the A15 Phase in Diblock Copolymer Melts. *Proc. Natl. Acad. Sci. U. S. A.* **2019**, *116*, 13194–13199.

(13) Grason, G. M.; DiDonna, B. A.; Kamien, R. D. Geometric Theory of Diblock Copolymer Phases. *Phys. Rev. Lett.* **2003**, *91*, 058304.

(14) Grason, G. M. The Packing of Soft Materials: Molecular Asymmetry, Geometric Frustration and Optimal Lattices in Block Copolymer Melts. *Phys. Rep.* **2006**, *433*, 1–64.

(15) Lee, S.; Leighton, C.; Bates, F. S. Sphericity and Symmetry Breaking in the Formation of Frank-Kasper Phases from One Component Materials. *Proc. Natl. Acad. Sci. U. S. A.* **2014**, *111*, 17723–17731.

(16) Chanpuriya, S.; Kim, K.; Zhang, J.; Lee, S.; Arora, A.; Dorfman, K. D.; Delaney, K. T.; Fredrickson, G. H.; Bates, F. S. Cornucopia of Nanoscale Ordered Phases in Sphere-Forming Tetrablock Terpolymers. *ACS Nano* **2016**, *10*, 4961–4972.

(17) Reddy, A.; Buckley, M. B.; Arora, A.; Bates, F. S.; Dorfman, K. D.; Grason, G. M. Stable Frank-Kasper Phases of Self-Assembled, Soft Matter Spheres. *Proc. Natl. Acad. Sci. U. S. A.* **2018**, *115*, 10233–10238.

(18) Luzzati, V.; Vargas, R.; Gulik, A.; Mariani, P.; Seddon, J. M.; Rivas, E. Lipid Polymorphism: A Correction. The Structure of the Cubic Phase of Extinction Symbol Fd--Consists of Two Types of Disjointed Reverse Micelles Embedded in a Three-Dimensional Hydrocarbon Matrix. *Biochemistry* **1992**, *31*, 279–285.

(19) Seddon, J. M.; Zeb, N.; Templer, R. H.; McElhaney, R. N.; Mannock, D. A. An *Fd3m* Lyotropic Cubic Phase in a Binary Glycolipid/ Water System. *Langmuir* **1996**, *12*, 5250–5253.

(20) Rappolt, M.; Cacho-Nerin, F.; Morello, C.; Yaghmur, A. How the Chain Configuration Governs the Packing of Inverted Micelles in the Cubic Fd3m-Phase. *Soft Matter* **2013**, *9*, 6291–6300.

(21) Shearman, G. C.; Tyler, A. I. I.; Brooks, N. J.; Templer, R. H.; Ces, O.; Law, R. V.; Seddon, J. M. A 3-D Hexagonal Inverse Micellar Lyotropic Phase. *J. Am. Chem. Soc.* **2009**, *131*, 1678–1679.

(22) Perroni, D. V.; Mahanthappa, M. K. Inverse Pm3n Cubic Micellar Lyotropic Phases from Zwitterionic Triazolium Gemini Surfactants. *Soft Matter* **2013**, *9*, 7919–7922.

(23) Martiel, I.; Sagalowicz, L.; Mezzenga, R. A Reverse Micellar Mesophase of Face-Centered Cubic Fm $\bar{3}$m Symmetry in Phosphatidylcholine/Water/Organic Solvent Ternary Systems. *Langmuir* **2013**, *29*, 15805–15812.

(24) Kim, K.; Schulze, M. W.; Arora, A.; Lewis, R. M.; Hillmyer, M. A.; Dorfman, K. D.; Bates, F. S. Thermal Processing of Diblock Copolymer Melts Mimics Metallurgy. *Science.* **2017**, *356*, 520–523.

(25) Baez-Cotto, C. M.; Mahanthappa, M. K. Micellar Mimicry of Intermetallic C14 and C15 Laves Phases by Aqueous Lyotropic Self-Assembly. *ACS Nano* **2018**, *12*, 3226–3234.

(26) Lindsay, A. P.; Lewis, R. M.; Lee, B.; Peterson, A. J.; Lodge, T. P.; Bates, F. S. A15, σ, and a Quasicrystal: Access to Complex Particle Packings via Bidisperse Diblock Copolymer Blends. *ACS Macro Lett.* **2020**, *9*, 197-203.

(27) Schulze, M. W.; Lewis, R. M.; Lettow, J. H.; Hickey, R. J.; Gillard, T. M.; Hillmyer, M. A.; Bates, F. S. Conformational Asymmetry and Quasicrystal Approximants in Linear Diblock Copolymers. *Phys. Rev. Lett.* **2017**, *118*. 207801.

(28) Lewis, R. M.; Arora, A.; Beech, H. K.; Lee, B.; Lindsay, A. P.; Lodge, T. P.; Dorfman, K. D.; Bates, F. S. Role of Chain Length in the Formation of Frank-Kasper Phases in Diblock Copolymers. *Phys. Rev. Lett.* **2018**, *121*. 208002.

(29) Roe, R. J.; Zin, W. C. Phase Equilibria and Transition in Mixtures of a Homopolymer and a Block Copolymer. 2. Phase Diagram. *Macromolecules* **1984**, *17*, 189–194.

(30) Kinning, D. J.; Winey, K. I.; Thomas, E. L. Structural Transitions from Spherical to Nonspherical Micelles in Blends of Poly(Styrene-Butadiene) Diblock Copolymer and Polystyrene Homopolymers. *Macromolecules* **1988**, *21*, 3502–3506.

(31) Kinning, D. J.; Thomas, E. L.; Fetters, L. J. Morphological Studies of Micelle Formation in Block Copolymer/ Homopolymer Blends. *J. Chem. Phys.* **1989**, *90*, 5806–5825.

(32) Winey, K. I.; Thomas, E. L.; Fetters, L. J. The Ordered Bicontinuous Double-Diamond Morphology in Diblock Copolymer/Homopolymer Blends. *Macromolecules* **1992**, *25*, 422–428.

(33) Hashimoto, T.; Koizumi, S.; Hasegawa, H.; Hyde, S. T. Observation of “Mesh” and “Strut” Structures in Block Copolymer / Homopolymer Mixtures. *Macromolecules* **1992**, 1433–1439.

(34) Spontak, R. J.; Smith, S. D.; Ashraf, A. Linear Multiblock Copolymer/Homopolymer Blends of Constant Composition. 1. Low-Molecular-Weight Homopolymers. *Macromolecules* **1993**, *26*, 5118–5124.

(35) Disko, M. M.; Liang, K. S.; Behal, S. K.; Roe, R. J.; Jeon, K. J. Catenoid-Lamellar Phase in Blends of Styrene-Butadiene Diblock Copolymer and Homopolymer. *Macromolecules* **1993**, *26*, 2983–2986.

(36) Floudas, G.; Hadjichristidis, N.; Stamm, M.; Likhtman, A. E.; Semenov, A. N. Microphase Separation in Block Copolymer/Homopolymer Blends: Theory and Experiment. *J. Chem. Phys.* **1997**, *106*, 3318–3328.

(37) Viadya, N. Y.; Han, C. D.; Do, K.; Sakamoto, N.; Hashimoto, T. Microdomain Structures and Phase Transitions in Binary Blends Consisting of a Highly Asymmetric Block Copolymer and a Homopolymer. *Macromolecules* **2001**, *34*, 222–234.

(38) Takagi, H.; Yamamoto, K.; Okamoto, S. Ordered-Bicontinuous-Double-Diamond Structure in Block Copolymer/Homopolymer Blends. *Eur. Phys. Lett.* **2015**, *110*, 48003.

(39) Takagi, H.; Hashimoto, R.; Igarashi, N.; Kishimoto, S.; Yamamoto, K. Frank–Kasper σ Phase in Polybutadiene-Poly(ε-Caprolactone) Diblock Copolymer/Polybutadiene Blends. *J. Phys. Condens. Matter* **2017**, *29*, 1–6.

(40) Takagi, H.; Yamamoto, K. Phase Boundary of Frank-Kasper σ Phase in Phase Diagrams of Binary Mixtures of Block Copolymers and Homopolymers. *Macromolecules.* **2019**, *52*, 2007–2014.

(41) Semenov, A. N. Phase Equilibria in Block Copolymer-Homopolymer Blends. *Macromolecules.* **1993**, 2273–2281.

(42) Likhtman, A. E.; Semenov, A. N. Theory of Microphase Separation in Block Copolymer/Homopolymer Mixtures. *Macromolecules* **1997**, *30*, 7273–7278.

(43) Matsen, M. W. Phase Behavior of Block Copolymer/Homopolymer Blends. *Macromolecules* **1995**, *28*, 5765–5773.

(44) Hashimoto, T.; Tanaka, H.; Hasegawa, H. Ordered Structure in Mixtures of a Block Copolymer and Homopolymers. 2. Effects of Molecular Weights of Homopolymers. *Macromolecules* **1990**, *23*, 4378–4386.

(45) Winey, K. I.; Thomas, E. L.; Fetters, L. J. Swelling a Lamellar Diblock Copolymer with Homopolymer: Influences of Homopolymer Concentration and Molecular Weight. *Macromolecules* **1991**, *24*, 6182–6188.

(46) Koizumi, S.; Hasegawa, H.; Hashimoto, T. Spatial Distribution of Homopolymers in Block Copolymer Microdomains As Observed by a Combined SANS and SAXS Method. *Macromolecules*. **1994**, *27*, 7893–7906.

(47) Kunieda, H.; Ozawa, K.; Huang, K.-L. Effect of Oil on the Surfactant Molecular Curvatures in Liquid Crystals. *J. Phys. Chem. B* **2002**, *102*, 831–838.

(48) Chen, L.; Lee, H. S.; Lee, S. Close-Packed Block Copolymer Micelles Induced by Temperature Quenching. *Proc. Natl. Acad. Sci. U. S. A.* **2018**, *115*, 7218–7223.

(49) Hynninen, A. P.; Thijssen, J. H. J.; Vermolen, E. C. M.; Dijkstra, M.; Van Blaaderen, A. Self-Assembly Route for Photonic Crystals with a Bandgap in the Visible Region. *Nat. Mater.* **2007**, *6*, 202–205.

(50) Jayaraman, A.; Zhang, D. Y.; Dewing, B. L.; Mahanthappa, M. K. Path-Dependent Preparation of Complex Micelle Packings of a Hydrated Diblock Oligomer. *ACS Cent. Sci.* **2019**, *5*, 619–628.

(51) Petříček, V.; Michal, D.; Lukáš, P. Crystallographic Computing System JANA2006: General Features. *Z.Kristallogr. Cryst. Mater*. **2014**, *229*, 245-352.

(52) Palatinus, L.; Chapuis, G. SUPERFLIP - A Computer Program for the Solution of Crystal Structures by Charge Flipping in Arbitrary Dimensions. *J. Appl. Crystallogr.* **2007**, *40*, 786–790.

(53) Yokoyama, H.; Kramer, E. J. Diffusion of Triblock Copolymers in a Spherical Domain Structure. *Macromolecules* **2000**, *33*, 954–959.

(54) Cavicchi, K. A.; Lodge, T. P. Self-Diffusion and Tracer Diffusion in Sphere-Forming Block Copolymers. *Macromolecules* **2003**, *36*, 7158–7164.

(55) Uddin, M. H.; Rodriguez, C.; Watanabe, K.; Lopez-Quintela, A.; Kato, T.; Furukawa, H.; Harashima, A.; Kunieda, H. Phase Behavoir and Formation of Reverse Cubic Phase Based Emlusion in Water/Poly(Oxyethylene) Poly(Dimethylsiloxane) Surfactants/Silicone Oil Systems. *Langmuir* **2001**, *17*, 5169–5175.

(56) Uddin, M. H.; Rodriguez, C.; Lopez-Quintela, A.; Leisner, D.; Solans, C.; Esquena, J.; Kunieda, H.; Graduate. Phase Behavior and Microstructure of Poly(Oxyethylene)-Poly(Dimethylsiloxane) Copolymer Melt. *Macromolecules* **2003**, *36*, 1261–1271.

(57) Zhao, M.; Li, W. Laves Phases Formed in the Binary Blend of AB_4 Miktoarm Star Copolymer and A-Homopolymer. *Macromolecules* **2019**, *52*, 1832–1842.

FOR TABLE OF CONTENTS USE ONLY